LETTER Communicated by Bard Ermentrout

Pattern Generation by Two Coupled Time-Discrete Neural Networks with Synaptic Depression

W. Senn
Th. Wannier
J. Kleinle
H.-R. Lüscher
L. Müller
J. Streit
K. Wyler
Universität Bern, Bühlplatz 5, CH-3012 Bern, Switzerland

Numerous animal behaviors, such as locomotion in vertebrates, are produced by rhythmic contractions that alternate between two muscle groups. The neuronal networks generating such alternate rhythmic activity are generally thought to rely on pacemaker cells or well-designed circuits consisting of inhibitory and excitatory neurons. However, experiments in organotypic cultures of embryonic rat spinal cord have shown that neuronal networks with purely excitatory and random connections may oscillate due to their synaptic depression, even without pacemaker cells. In this theoretical study, we investigate what happens if two such networks are symmetrically coupled by a small number of excitatory connections. We discuss a time-discrete mean-field model describing the average activity and the average synaptic depression of the two networks. Depending on the parameter values of the depression, the oscillations will be in phase, antiphase, quasiperiodic, or phase trapped. We put forward the hypothesis that pattern generators may rely on activity-dependent tuning of synaptic depression.

1 Introduction

Spinal pattern generators rely on intrinsic spinal circuits activated by descending signals from the brain stem that autonomously coordinate the alternate rhythmic activity inducing walking or swimming. The basis of the alternate oscillations is thought to consist of reciprocal inhibitory synaptic interactions between two groups of neurons (Getting, 1989). We suggest that this same functionality can be realized by depressing synapses with purely excitatory connections between and within the two neural groups. The proposed mechanism for pattern generation seems to be particularly attractive since in the early stage of prenatal development, the inhibitory connections are not yet developed but rhythmic activity can already be

observed (Gao & Ziskind-Conhaim, 1995). Moreover, the transition between different activity patterns does not need to be tuned by descending input or additional circuits. Rather, these transitions may be induced by changing the parameters controlling the dynamics of the synaptic depression without affecting the connection strength between the networks. The synaptic parameters themselves can be thought of as being activity dependent, and this will allow the spinal cord to recall different rhythmic patterns in a self-organizing way. An activity-dependent regulation of synaptic depression has indeed been found experimentally in other regions of the nervous system (Markram & Tsodyks, 1996; Abbott, Varela, Sen, & Nelson, 1997), and current network simulations suggest that this synaptic self-regulation may indeed be necessary to generate spinal cord oscillations in a narrower physiological parameter regime (Streit & Senn, 1997).

In embryonic rat spinal cord cultures, rhythmical activities are induced by pharmacological blockage of inhibitory synaptic transmissions (Streit, 1993). A time-discrete mathematical model has been developed to investigate the observed phenomena, and its analysis has shown that rhythmical activities characterized by the synchronous firing of numerous neurons can be obtained from randomly connected excitatory neurons with synaptic depression (Senn et al., 1996). However, it is not clear whether the alternating activity typical for spinal pattern generators can also be based on such mechanisms. To analyze this question, we investigated the activity generated by a symmetrical coupling between two identical networks (called *isotropic* coupling), as it may occur between the two sides of the spinal cord. We describe the state of a network by two time-dependent variables: the average activity and the average synaptic depression. Guided by observations in organotypic cultures of embryonic rat spinal cord, the strength of synaptic transmission between two neurons is taken to be depressed after the occurrence of an action potential in the presynaptic cell and to return to its normal value with an exponential time course. We found that the time constant of the recovery from synaptic depression is an adequate parameter to control the dynamics of the coupled system. In the spinal slice cultures, the time constant of synaptic depression could be pharmacologically modulated by atropin, leading to the speculation of a physiological modulation by presynaptic receptors. Depending on this time constant, the activities of the networks will either converge to a fixed value or show various types of rhythmic behavior. We observe the following oscillations in the two networks: inphase (0 degree phase lag), antiphase (180 degree phase lag), out-of-phase (constant phase lag other than 0 or 180 degrees), quasiperiodic (oscillating amplitudes), phase trapped (oscillating phase lag), or phase walkthrough (constant phase drift). In addition, we find bistability where both inphase and antiphase oscillations are stable at the same parameter values.

Coupled neural oscillators have been studied theoretically in different contexts. They have been found to occur in the locomotion of the lamprey

(Kopell, 1988), in circadian rhythms (Kawato & Suzuki, 1980), in paired cell oscillations (Rinzel & Ermentrout, 1989; Sherman & Rinzel, 1992), in short-term memory (Horn & Usher, 1991), and more recently in elementary pattern recognition where they serve for dynamic feature binding and pattern segmentation (Gerstner, Ritz, & van Hemmen, 1993; Wang & Terman, 1997). In the light of the recent discoveries of synaptic depression in neocortex (Markram & Tsodyks, 1996; Abbott et al., 1997), one can ask whether the different oscillation patterns that could emerge from synaptic depression also play a role in higher cognitive functions.

From a mathematical point of view, coupled oscillators are classified according to the strength of coupling, and different techniques have been developed for different coupling strengths. If the coupling is weak, the effect of the coupling depends on only the phase difference between the oscillators. This approach of reducing each oscillator to a single-phase variable is based on the average phase difference (APD) theory (Ermentrout & Kopell, 1991), which until now has been used only in the context of time-continuous systems. By applying these ideas to the time-discrete case, we can explain phase-locking phenomena such as inphase and antiphase oscillations (section 3). Unlike the time-continuous case where only phase-locked solutions exist for isotropically coupled oscillators of the same frequency, phase trapping is also possible in the time-discrete case. If the coupling becomes stronger, the amplitudes of the oscillations are disturbed as well, and quasiperiodicity can occur in both cases. The technique for investigating this stronger coupling is bifurcation analysis, which we apply to the time-discrete model (section 4).

2 The Model

A neuron is considered to be a threshold element producing an action potential when the sum of incoming excitatory postsynaptic potentials (EPSPs) exceeds some defined threshold value (see Figure 1a). The number of (excitatory) synaptic connections projecting onto each of a population of cells is assumed to be Poisson distributed with mean μ. Thus, the probability that there are m connections onto a specific cell is $\frac{\mu^m}{m!}e^{-\mu}$. This probability is assumed to be the same for each cell in the network, a reasonable assumption as long as one considers cultures of embryonic spinal cord. Although there are on average μ anatomical connections ending up on a single cell, only a fraction of these synaptic connections is functionally active and may induce an EPSP in the postsynaptic cell. Obviously the presynaptic cell must be active, but at the same time, the synaptic transmission must function reliably. On average, the number of active connections is reduced to $\mu a_t s_t$, where $a_t \in [0, 1]$ is the average activity of cells and $s_t \in [0, 1]$ is the average synaptic reliability at time t. Thus, the probability that there are m active connections projecting onto a cell at time t is $\frac{(\mu a_t s_t)^m}{m!}e^{-\mu a_t s_t}$. If a cell needs $m_\circ$

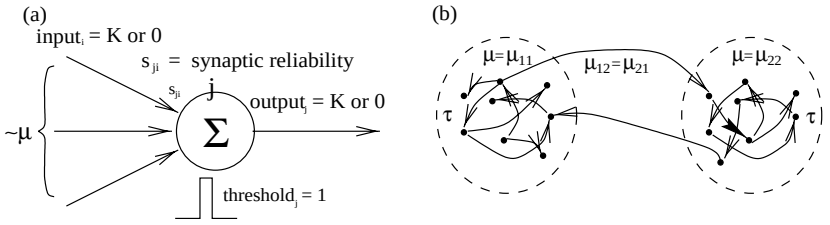

Figure 1: (a) Each neuron is modeled by a threshold element with time-dependent synaptic reliability. The number of connections onto cell j is Poisson distributed with mean μ. A possible action potential from cell i to cell j is transmitted only with reliability $s_{ji} \in [0, 1]$. (b) Two weakly coupled networks with random excitatory connections.

incoming EPSPs to exceed a set threshold, the probability of triggering an action potential at time $t + 1$ becomes

$$\sum_{m \geq m_\circ} \frac{(\mu a_t s_t)^m}{m!} e^{-\mu a_t s_t} = \frac{1}{\Gamma(m_\circ)} \int_0^{\mu a_t s_t} x^{m_\circ - 1} e^{-x}\, dx \; .$$

The equation is obtained by integrating the right-hand side $m_\circ - 1$ times by parts.

If the threshold is normalized to 1 and if K represents the height of an average EPSP, the cell needs at least $m_\circ = \frac{1}{K}$ EPSPs to reach threshold. The average activity a_{t+1} of the whole network at time $t + 1$ is equal to the probability that any single cell is activated. Thus,

$$a_{t+1} = F_K(\mu a_t s_t), \qquad \text{where } F_K(y) \doteq \frac{1}{\Gamma(\frac{1}{K})} \int_0^y x^{\frac{1}{K}-1} e^{-x}\, dx \; . \tag{2.1}$$

In the embryonic spinal cord cultures of the rat, an EPSP is found to be very large and is roughly 0.8 times threshold (which itself is ~ 13 mV above the resting potential; Streit, 1993). We therefore fix the height of an undepressed EPSP at $K = 0.8$. In the same cultures, the average number of connections is estimated to lie between 3 and 20. The average conduction delay between two cells is ~ 14 ms, and this time delay is assumed to elapse between time step t and $t+1$ in our model (Streit, Spenger, & Lüscher, 1991). The long conduction delay is explained by the immaturity of the cells and the fact that axons are not myelinated.

The average synaptic reliability s_{t+1} is calculated from its value s_t and the average activity a_t at the previous time step. Due to effects of synaptic depression, s_{t+1} becomes small if the previous activity a_t was large. The synaptic reliability will therefore be depressed by a factor $d_\tau(a_t)$, where $d_\tau(y) \doteq 1 - ye^{-\frac{1}{\tau}}$ is a linearly decreasing function in y. The constant τ is

interpreted as the time constant of recovery from synaptic depression and is referred to as the synaptic depression time (constant). It has been found to be $\sim$220 ms (Streit et al., 1991), which corresponds to 15 time steps in our model. In addition, due to synaptic recovery effects, the synaptic reliability s_{t+1} should be small if it was small during the previous time step. This is expressed by a further depression factor $d_\tau(1 - s_t)$, a linearly increasing function of s_t. Including both effects, the synaptic reliability s_t is given by

$$s_{t+1} = d_\tau(a_t) \cdot d_\tau(1 - s_t), \qquad d_\tau(y) = 1 - y \cdot e^{-\frac{1}{\tau}}. \tag{2.2}$$

This same formula can also be derived by looking at the history of a single synapse and a subsequent averaging over the ensemble. Let $s_{ji}(t)$ be the individual synaptic reliability of the connection from cell i to cell j at time t. As a function of the activity of the presynaptic cell i during the past two time steps $t-1$ and $t-2$, we set

$$s_{ji}(t) = \begin{cases} 1, & \text{if cell } i \text{ was active at neither time } t-2 \text{ nor } t-1 \\ 1 - e^{-\frac{2}{\tau}}, & \text{if cell } i \text{ was active at time } t-2 \text{ but not at } t-1 \\ 1 - e^{-\frac{1}{\tau}}, & \text{if cell } i \text{ was active at time } t-1 \text{ but not at } t-2 \\ (1 - e^{-\frac{1}{\tau}})(1 - e^{-\frac{2}{\tau}}), & \text{if cell } i \text{ was active at time } t-1 \text{ and } t-2\ . \end{cases} \tag{2.3}$$

The idea is to quantify the influence of a synaptic transmission that occurred $\triangle t$ time steps before by depressing $s_{ji}(t)$ with a factor $(1 - e^{-\triangle t/\tau})$. Taking into account only the two preceding time steps and averaging over i and j yields, together with the first-order approximation $s_{t-1} \approx 1 - a_{t-2}e^{-1/\tau}$, the final formula, equation 2.2 (cf. Senn et al., 1996).

We now consider two networks with identical parameter values that are weakly symmetrically coupled in both directions (see Figure 1b). The average number of (excitatory) connections between cells of network i and j is denoted by $\mu_{ji} = \mu_{ij}$ $(i, j \in \{1, 2\},\ i \neq j)$. The number of connections between the networks is again assumed to be Poisson distributed with mean μ_{ij}. Thus, the average number of connections active at time t and terminating on a cell of the population i consists of active connections of its own population and of the other population and sums to $\mu_{ii}a_t^i s_t^i + \mu_{ij}a_t^j s_t^j$. Here, a_t^i and s_t^i $(i = 1, 2)$ denote the average activity and the average synaptic reliability, respectively, of population i. From equations 2.1 and 2.2, we obtain the time-discrete evolution of the coupled system:

$$\begin{aligned} a_{t+1}^1 &= F_K(\mu a_t^1 s_t^1 + \mu_{12} a_t^2 s_t^2), & a_{t+1}^2 &= F_K(\mu a_t^2 s_t^2 + \mu_{21} a_t^1 s_t^1), \\ s_{t+1}^1 &= d_\tau(a_t^1) \cdot d_\tau(1 - s_t^1), & s_{t+1}^2 &= d_\tau(a_t^2) \cdot d_\tau(1 - s_t^2). \end{aligned} \tag{2.4}$$

In the following discussion, we qualitatively distinguish between weak coupling, which essentially affects only the phases and frequencies of the individual oscillators, and medium-strength coupling, which also influences their amplitudes. In the scenario of weak coupling, we set the average number μ_{ij} of connections between cells of different networks to ~ 0.001 (compare this to the typical number $\mu \sim 10$ of intrinsic connections per cell), and for medium-strength coupling we set it to 0.1. It is also possible for pairs of networks to be strongly coupled, where μ_{ij} is larger than ~ 1. Such oscillators produce only in-phase oscillations.

3 Weak Coupling: Average Phase Difference Theory

3.1 Average Phase Difference Theory for Discrete Time. In APD theory, the description of an oscillator is reduced to a single phase variable. This phase corresponds to the angle that fixes the position of the oscillator on the closed curve representing the dynamics in phase space (cf. Figure 10b). The interaction of two oscillators is then studied by its influence on the phase difference between the oscillators. In the following, we apply this theory, which originally was developed for continuous time (Kopell, 1988), to the present case of discrete time.

We assume that the mapping $(a_t, s_t) \rightarrow (a_{t+1}, s_{t+1})$ of the uncoupled system is smooth and that there is a stable invariant closed curve describing the uncoupled oscillator. We also assume that the uncoupled mapping is transformed in such a way that on the closed curve, it shows a constant increment of the phase $\theta_t, \theta_{t+1} - \theta_t = \omega$. This is always possible if the rotation number $\omega/2\pi$ of the invariant closed curve is irrational (Guckenheimer & Holmes, 1990; Denjoy's theorem). The constant ω is interpreted as the radial frequency of the phase-variable θ. (Note that the radial frequency ω can be negative, while the natural frequency $f = |\omega|/2\pi$ of the oscillator is always positive.) Now we consider two weakly symmetrically coupled identical oscillators with smooth coupling function $h^\epsilon(\theta_t^i, \theta_t^j)$ with

$$0 < |h^\epsilon| \leq \epsilon \ll 1 \,. \tag{3.1}$$

The coupling is supposed to change the (instantaneous) radial frequency ω of oscillators i by some quantity h^ϵ, depending on the actual phases θ_t^i and θ_t^j of oscillator i and j, respectively. The function $h = h^\epsilon(\theta_t^i, \theta_t^j)$ defined this way describes the acceleration of the frequency of oscillator i during one time step caused by the coupling. Thus, the equations $\triangle\theta_t^i \equiv \theta_{t+1}^i - \theta_t^i = \omega$, $(i = 1, 2)$, of the uncoupled system become in the presence of symmetric coupling:

$$\triangle\theta_t^1 = \omega + h^\epsilon(\theta_t^1, \theta_t^2), \quad \triangle\theta_t^2 = \omega + h^\epsilon(\theta_t^2, \theta_t^1). \tag{3.2}$$

If ϵ is small, the phase difference between the two oscillators does not change too much during n ($\gg 1$) iterations as long as $n \ll 1/\epsilon$. Moreover, if $\omega/2\pi$ is

irrational, the iterated points $\theta_0^i = 0\,, \theta_1^i \approx \omega\,, \theta_2^i \approx 2\omega, \ldots, \theta_n^i \approx n\omega$ start to sample the invariant curve (ϵ-)densely and (ϵ-)uniformly, and this allows averaging the coupling effect over the closed curve. Hence, dropping the index ϵ, the average influence of the coupling at phase lag ϕ is approximately

$$H(\phi) = \frac{1}{2\pi} \int_0^{2\pi} h(\theta, \theta + \phi)\, d\theta, \tag{3.3}$$

and this represents the average acceleration per time step of one oscillator if it lags the other by ϕ. For a numerical evaluation of the function H, we refer to section A.1 (an algorithm in the time-continuous case is presented in Williams & Bowtell, 1997). The average phase increments of the two isotropically coupled oscillators may now be written as

$$\triangle\theta_t^1 = \omega + H(\phi_t), \quad \triangle\theta_t^2 = \omega + H(-\phi_t), \tag{3.4}$$

where $\phi_t = \theta_t^2 - \theta_t^1$. The condition that the two oscillators are phase locked is $\phi_{t+1} - \phi_t = 0$. From equation 3.4, one calculates

$$\phi_{t+1} - \phi_t = \triangle\theta_t^2 - \triangle\theta_t^1 = H(-\phi_t) - H(\phi_t) = -2H_{odd}(\phi_t) = 0, \tag{3.5}$$

where $H_{odd}(\phi) \doteq \frac{1}{2}(H(\phi_t) - H(-\phi_t))$ denotes the antisymmetric part of H. Thus, two solutions θ_t^1 and θ_t^2 are phase locked with constant phase lag $\phi_\circ$ if and only if $H_{odd}(\phi_\circ) = 0$. The solutions are stably phase locked if, for any small deviation ϕ_t from $\phi_\circ$, the successive phase lags ϕ_{t+1}, $\phi_{t+2}, \ldots$ converge back to $\phi_\circ$. It is a simple result from the iteration theory of real functions that a function $\phi_{t+1}(\phi_t)$ is stable at $\phi_\circ$ if it crosses the diagonal $\phi_{t+1} = \phi_t$ with an angle less than 45 degrees—that is, if $|\frac{d\phi_{t+1}}{d\phi_t}| < 1$ at this point (consider Figure 1b in Senn et al., 1996, with a replaced by ϕ, or consider the standard book of Collet & Eckmann, 1986). According to equation 3.5, one has $\phi_{t+1} = \phi_t - 2H_{odd}(\phi_t)$, and the last equality turns out to be equivalent to

$$0 < \left.\frac{dH_{odd}(\phi)}{d\phi}\right|_{\phi=\phi_\circ} < 1\,. \tag{3.6}$$

Thus, equation 3.6 is the condition that the two oscillators, locked at lag $\phi_\circ$, are actually stably locked. Notice that the upper bound is due to the time discretization and does not occur for continuous time (Kopell, 1988, formula 3.7). To make a rigorous statement, we must restrict ourselves to rotation numbers $\omega/2\pi$, which are *badly approximated* by rational numbers—that is, which satisfy for some $c, \nu > 0$ the relation

$$\left|\frac{\omega}{2\pi} - \frac{p}{q}\right| \geq \frac{c}{q^{2+\nu}} \quad \text{for all } p \in \mathbf{Z} \text{ and } q \in \mathbf{N}\,. \tag{3.7}$$

This condition is necessary to exclude a self-locking of the coupled oscillators on a rational frequency, which could make the approximation in equation 3.3 bad. Our investigations lead to the following theorem:

Theorem 1. *Suppose the mapping describing the uncoupled system exhibits a stable invariant closed curve with rotation number* $\omega/2\pi \in \mathbf{R} \setminus \mathbf{Q}$ *being badly approximated by rationals. We assume a coupling of the form in equation 3.2 with coupling function* h^ϵ *satisfying equation 3.1. Then, for small* ϵ*, the dynamics of the coupled system in equation 3.2 is approximated by the averaged equations (see equation 3.4). The number of phase-locked solutions of equation 3.4 is even and, enumerating them according to increasing phase lag, at most, every second of these solutions is stably phase locked. If there are exactly two phase-locked solutions, the corresponding phase lags must be* $\phi_\circ = 0$ *and* $\phi_\circ = \pi$*, and at least one of them is unstable. A solution locked at lag* $\phi_\circ$ *is stable if and only if equation 3.6 is satisfied. The change of the radial frequency* ω *from the uncoupled oscillation to the phase-locked oscillation is approximately given by* $H(\phi_\circ)$.

Remark. The restriction of $\omega/2\pi$ to numbers that are badly approximated by rational numbers is rather severe since, although these numbers have full measure, the parameter values leading to an invariant curve with rational rotation number generically form open-dense sets (the so-called Arnold tongues; cf. Arnold, 1965) in the parameter space. On the other hand, the parameter values with irrational rotation numbers generically have positive measure as well (Herman, 1983; Guckenheimer & Holmes, 1990).

Proof of Theorem 1. Since the uncoupled mapping exhibits an invariant curve, it is possible to define the coupling function $h^\epsilon(\theta_t^i, \theta_t^j)$ together with its average $H(\phi)$ (cf. section A.1). If the rotation number $\omega/2\pi$ of the uncoupled mapping is irrational, the angles $\theta_t = t\,\omega + \theta_\circ$ $(t = 1, 2, \ldots)$ of the uncoupled system are uniformly distributed (see, e.g., Hlawka, 1979) and for small ϵ, the temporal average of the interactions converges to the spatial average $H(\phi)$ in the same way as this is the case for multiple-pulse-coupled oscillators (Ermentrout & Kopell, 1991). In the time-discrete case, we are faced with the additional problem that the single oscillator might be self-locked onto a fixed frequency and a fixed phase and that this self-locking force could dominate the influence of the coupling between the two networks. It remains to be proved in a mathematically rigorous way that if $\omega/2\pi$ is badly approximated by rationals, the self-locking can be excluded, since for small perturbations, the locking at the frequency $\omega/2\pi$ is of lower order than the interaction h^ϵ (cf. Arnold, 1965). For small ϵ, the qualitative dynamics of the coupled system in equation 3.2 will then be the same as for the averaged system in equation 3.4.

To discuss the approximation in equation 3.4, we note that according to equation 3.5, every zero $\phi_\circ$ of H_{odd} leads to a phase-locked solution of

equation 3.4, and $\phi_\circ$ represents the constant phase lag from the first to the second oscillator. Now, the origin $\phi_\circ = 0$ is always a zero of H_{odd} since H_{odd} is antisymmetrical, that is, $H_{odd}(-\phi) = -H_{odd}(\phi)$. Similarly, $\phi_\circ = \pi$ is always a zero since H_{odd} is antisymmetrical with respect to π, that is, $H_{odd}(\pi - \phi) = -H_{odd}(\pi + \phi)$. This last equation follows from the antisymmetry (with respect to 0) and the 2π periodicity of H_{odd}. But the antisymmetry with respect to π implies that every zero must occur symmetrically to π. Since these zeros are generically nondegenerate (i.e., $H'_{odd}(\phi_\circ) \neq 0$; see above), every new zero appears pairwise in the interval $(0, 2\pi)$ (cf. Figure 2b). To prove the stability statements, one asserts that generically at every second zero, the function H_{odd} crosses the zero line with positive slope. According to the criterion in equation 3.6, an upward crossing corresponds to a stably phase-locked solution if, in addition, the slope is < 1. Thus, at most every second zero can be stable. In case of exactly two zeros (which must be 0 and π) either the inphase, the antiphase, or neither is stable. The statement about the frequency follows directly from equations 3.4, from which the frequency of an oscillation locked at lag $\phi_\circ$ is found to be $\omega + H(\phi_\circ)$.

Apart from the restriction imposed onto the rotation number, there is another important difference between APD theory for discrete and continuous time. For continuous time, the phase-locked solutions for isotropic coupling generically arise in pairs symmetrically to the zero lag. Since for continuous time the stability criterion does not include the upper bound in equation 3.6, there is generically at least one attractive phase lag, and any oscillation will eventually stably phase-lock. For discrete time, however, the phase-locked solutions may all be unstable since there is no guarantee that every second zero of H will also satisfy the upper bound in equation 3.6. In such a case, the phase either waxes and wanes (phase trapping) or shows a constant drift (phase walkthrough). Thus, two weakly isotropically coupled time-discrete oscillators will, after some transient, be either phase locked, phase trapped, or phase walkthrough. In case of phase trapping, the phase lag can show any dynamical behavior known from iteration theory of one-dimensional maps such as 2^k periodicity, almost periodicity, and chaos (Collet & Eckmann, 1986). For continuous time, phase-trapped solutions were first investigated by Wever (1972) and Kronauer, Czeisler, Pilato, Moore-Ede, & Weitzman (1982) by means of an additional amplitude consideration.

3.2 Application of APD Theory to the Time-Discrete Model. In order to apply the theorem to the system (see equation 2.4) we have to ensure that the rotation number of the uncoupled oscillation (μ_{ij}) is irrational. This is the case if the limit set of an iterated point of the uncoupled system forms a closed curve in the (a, s)-phase plane. It turns out that for the mapping, there is indeed a high chance of finding parameter values (μ, τ, K) with such an invariant closed curve. According to the remark above, there is always a nonvanishing chance to get an irrational rotation number by randomly

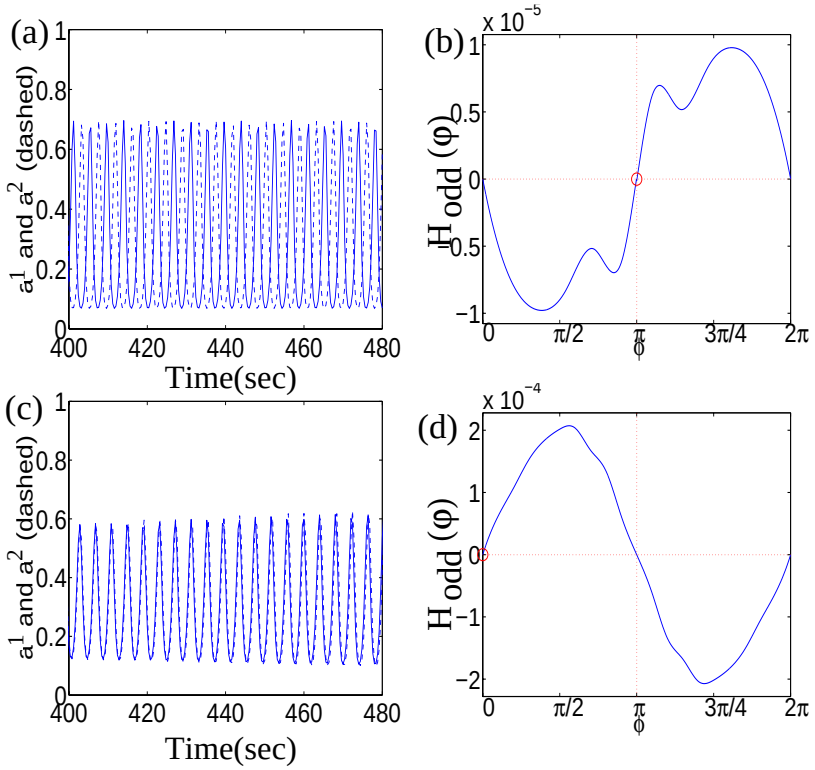

Figure 2: A zero $\phi_\circ$ of the function H_{odd} represents stable oscillations with phase lag $\phi_\circ$. (a,b) For very weak coupling strength $\mu_{ij} = 0.0001$ the phase lag $\phi_\circ = \pi$ satisfies the stability criterion (see equation 3.6), and the antiphase oscillation is therefore stable. (c,d) For weak coupling with $\mu_{ij} = 0.02$ the slope of H_{odd} is positive at the zero $\phi_\circ = 0$, and the in-phase oscillation is now stable.

choosing the parameter values. The chance to pick out "bad" parameter values from an Arnold tongue, which then lead to a discrete orbit with a rational rotation number is smaller the weaker the coupling is.

As an example, we consider the uncoupled system for the parameter values $\mu = 9.0$, $\tau = 9.5$, and $K = 0.8$ and calculate the function $H(\phi)$ for the two coupling strengths $\mu_{ij} = 0.0001$ and $\mu_{ij} = 0.02$ (see Figures 2b and 2d and section A.1 for more details). Looking at the zeros of the asymmetric part H_{odd} shows that in both cases, there are phase-locked solutions at $\phi_\circ = 0$ and $\phi_\circ = \pi$. However, applying the criterion in equation 3.4, only the antiphase solution at coupling strength $\mu_{ij} = 0.0001$ (see Figure 2b, $\phi_\circ = \pi$) and the inphase solution at $\mu_{ij} = 0.02$ (see Figure 2d, $\phi_\circ = 0$), for which the

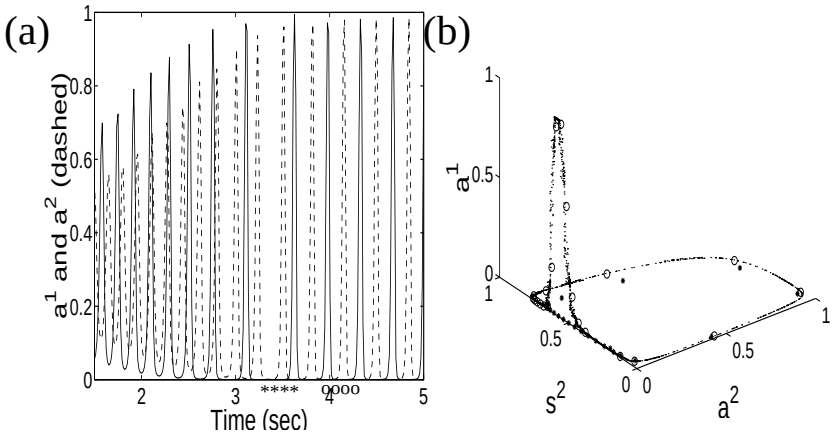

Figure 3: (a) One network may "stumble" and oscillate twice in a silent period of the other ($\mu = 10$, $\tau = 12$, $\mu_{ij} = 0.002$). (b) The corresponding phase diagram (a^1, a^2, s^2) shows that the trajectory cuts off the blob of the a^1-oscillation during the time from 3.3–3.6 s (marked with $***$ in *a* and *b*) while for 3.9–4.2 s, the trajectory follows the invariant curve ($\circ\circ\circ$).

slope of H_{odd} at the zero is positive, are stably phase locked. Starting at the same initial condition, the system will converge after some transients to a stable antiphase oscillation (see Figure 2a) or to a stable in-phase oscillation (see Figure 2b). For some intermediate values of the coupling strength, the function H_{odd} will cross the $\phi-$axes at phase lags different from 0 and π, and out-of-phase oscillations with stable lags $\phi_\circ \neq 0, \pi$ can be observed. In general, increasing the coupling strength tends to stabilize the in-phase solution.

An interesting anomaly is discovered for some parameter values, which we call a *stumbling solution*. For these parameter values, one may have two oscillations of one network against one oscillation of the other network. After a transient period, the network eventually will phase-lock (see Figure 3).

4 Medium-Strength Coupling: A Bifurcation Analysis

If the coupling strength is increased by two orders of magnitude, we find new phenomena such as bistability (stable inphase and antiphase oscillations) and quasiperiodicity (oscillating amplitude). To explain these phenomena, we fix the coupling strength between the networks at $\mu_{ij} = 0.1$ and discuss the bifurcations induced by changing the synaptic depression time τ and the coupling strength μ within the networks. First we transform

the system of coupled oscillators into appropriate coordinates to study the inphase and antiphase oscillations. This canonical transform is given by the linear mapping $(a_t^1, s_t^1, a_t^2, s_t^2) \overset{S}{\longmapsto} (a_t^+, s_t^+, a_t^-, s_t^-)$, where

$$\begin{aligned} a_t^+ &\doteq \frac{a_t^1 + a_t^2}{2}, \quad s_t^+ \doteq \frac{s_t^1 + s_t^2}{2} \\ \text{and} \\ a_t^- &\doteq \frac{a_t^1 - a_t^2}{2}, \quad s_t^- \doteq \frac{s_t^1 - s_t^2}{2}. \end{aligned} \tag{4.1}$$

Analyzing the steady-state equations of system 2.4, we can show that there is at most one attracting fixed point within the open cube $(0, 1)^4$. This fixed point has the coordinates (P_{fix}, P_{fix}), where $P_{fix} = (a_\circ, s_\circ)$ is the "second" intersection point of the nullclines $C_{K,\mu+\mu_{ij}} = \{(a, s) \mid a = F_K((\mu + \mu_{ij})as)\}$ and $C_\tau = \{(a, s) \mid s = d_\tau(a)d_\tau(1 - s)\}$ (see Senn et al., 1996).

For in-phase solutions, the coordinates a^- and s^- vanish, while for ("pure") antiphase solutions, one has $a_t^+ = a_\circ$ and $s_t^+ = s_\circ$ for all t. The fixed point within these new coordinates is $S((P_{fix}, P_{fix})) = (P_{fix}, \mathbf{0})$. Let $\Phi : (a_t^+, s_t^+, a_t^-, s_t^-) \longmapsto (a_{t+1}^+, s_{t+1}^+, a_{t+1}^-, s_{t+1}^-)$ be the mapping (see equation 2.4) in the new coordinates. The crucial point is that the linearization of Φ at the fixed point diagonalizes to

$$d\Phi|_{(P_{fix},\mathbf{0})} = \begin{pmatrix} d\Phi^+ & 0 \\ 0 & d\Phi^- \end{pmatrix}, \tag{4.2}$$

where $d\Phi^\pm$ are 2×2 matrices (cf. section A.2). The tangent space decomposes into a direct sum $E^+ \oplus E^- \simeq \mathbf{R}^2 \times \mathbf{R}^2$ on which $d\Phi^+$ and $d\Phi^-$ act, respectively. E^+ is the space of the in-phase solutions and is spanned by the coordinates (a^+, s^+) while E^- is the space of the antiphase solutions and is spanned by (a^-, s^-) and translated to the fixed point. The stability of the fixed point within the subspaces E^+ and E^- is determined by the stability of the corresponding restricted tangent mappings $d\Phi^\pm$. These linear mappings are stable if their eigenvalues have modulus smaller than 1 and unstable if the modulus is larger than 1. As shown in section A.2, the eigenvalues of $d\Phi^+$ and $d\Phi^-$, denoted by λ^+, $\overline{\lambda^+}$ and λ^-, $\overline{\lambda^-}$, respectively, are complex conjugates and their modulus is calculated as

$$|\lambda^\pm| = \sqrt{(\mu \pm \mu_{ij})\eta\epsilon_\tau(s_\circ + (1 - \epsilon_\tau)a_\circ)}, \tag{4.3}$$

where we abbreviated

$$\begin{aligned} \eta &\doteq f_K((\mu + \mu_{ij})a_\circ s_\circ)\ , \ \ f_K(y) \\ &\doteq \frac{1}{\Gamma(1/K)} y^{\frac{1}{K}-1} e^{-y} \ \text{ and } \quad \epsilon_\tau = e^{-\frac{1}{\tau}}. \end{aligned} \tag{4.4}$$

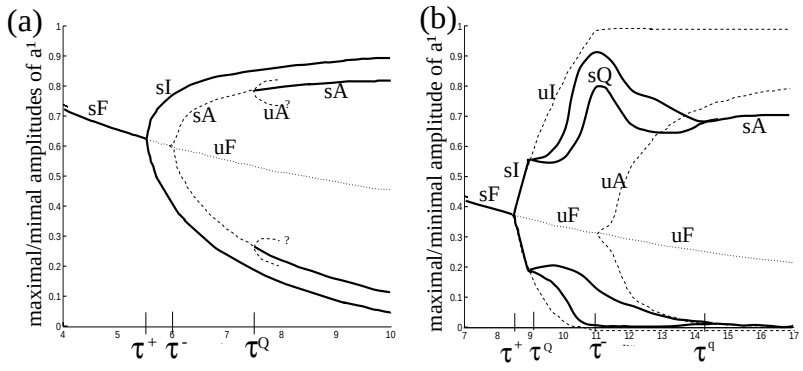

Figure 4: (a) Bifurcation diagram for $\mu = 16$. (b) Bifurcation diagram for $\mu = 10$. At τ^+ and τ^- a Naimark-Sacker bifurcation in the plane E^+ and E^-, respectively, occurs. At τ^Q, the invariant circle bifurcates into an invariant torus, which again merges into a circle at τ^q. The following abbreviations are used: s = stable, u = unstable, F = fixed point, I = in-phase oscillation, A = antiphase oscillation, Q = quasiperiodic oscillation.

4.1 Bifurcations with Respect to the Depression Time Constant τ. By tuning the synaptic depression time τ, we find that $|\lambda^-| < 1$ and $|\lambda^+| < 1$ for τ smaller than some critical value τ^+ (see Figures 4a and 4b). This shows that the fixed point is stable for $\tau < \tau^+$. At $\tau = \tau^+$ the eigenvalue λ^+ crosses the unit circle and generates a (forward, supercritical) Naimark-Sacker bifurcation (the discrete analog of a Hopf bifurcation for flows) in the subspace E^+. From this bifurcation, a stable invariant curve C^+ close to the subspace E^+ emerges, and this curve is composed of all in-phase solutions with different starting values. There is a second Naimark-Sacker bifurcation if the fixed point loses its stability in the directions of E^- as well. This happens at $\tau = \tau^-$ when the eigenvalue λ^- crosses the unit circle (see Figures 4a and 4b). At this point, an invariant curve C^- emerges within E^-, which comprises the antiphase solutions for different starting values. At its birth, when C^- is still near the fixed point, C^- is unstable since the fixed point is unstable in the directions E^+ orthogonal to C^-.

In the case $\mu = 16$ (see Figure 4a), C^- and thus the antiphase solutions become stable at some value $\tau^Q > \tau^-$ (e.g., through a backward torus bifurcation, which was not clearly identified numerically). Independent of this stability change of the antiphase solutions, the in-phase solution remains stable for all values $\tau > \tau^+$. As the bifurcation diagram (see Figure 4a) shows, we have bistability, in other words, the stability of the in-phase and antiphase oscillations at the same parameter values. Figure 5 shows that for $\tau = 9$, both solutions may stabilize after a few oscillations. If the synaptic

depression time τ is increased also, first the in-phase and then the antiphase cycle disappear, and this leads to the extinction of any activity.

Fixing the connectivity parameter at $\mu = 10$ (see Figures 4b and 6), we further observe a bifurcation of the stable invariant curve C^+ into a stable invariant 2-torus. This occurs at parameter value $\tau = \tau^Q$, where C^+ itself loses its stability. The limit set of a trajectory then consists of either the 2-torus itself (as for $\tau = 10$ in Figure 6), a finite number of closed curves (see Figure 7a), or a finite number of points. These different limit sets arise if the components of the corresponding rotation vector $(\omega^1/2\pi, \omega^2/2\pi)$ are both irrational (2-torus), if one is irrational and the other rational (collection of closed curves), or if both are rational (collection of isolated points). Here, ω^1 and ω^2 are the radial frequencies of the activity oscillations and the slower amplitude oscillations, respectively. The phenomenon of having two oscillations with different time scales is sometimes referred to as quasiperiodicity. Between $\tau = 11$ and $\tau = 12$, the 2-torus splits again and forms a 3-torus (not shown in the bifurcation diagram) since we find three frequencies corresponding to a rotation vector $(\omega^1/2\pi, \omega^2/2\pi, \omega^3/2\pi)$ (see Figure 7b). The three different frequencies represent the fast frequency of the original oscillation ($\sim$6.3 Hz), the slower frequency of the amplitude oscillations ($\sim 3 \cdot 10^{-2}$ Hz), and the slowest frequency of the amplitude-bound oscillations ($\sim 3 \cdot 10^{-4}$ Hz). In the phase space, the corresponding trajectory moves on a 3-torus isomorphic to the direct product of three circles. If only the first two oscillations are present, the trajectory lies on a 2-torus embedded in $[0, 1]^4$ (see Figure 7a). Examining the oscillations in Figure 7b more closely, one sees that the two solutions are phase trapped; the phase difference itself may oscillate (see Figure 8a). At $\tau = \tau^q$, the attracting 2-torus collapses to a stable cycle, which now represents a stable alternating oscillation (as for $\tau = 15$ in Figure 6). Figure 8b shows that the different oscillation types found for static values of τ are also present if the parameter τ is increased dynamically. For mathematical correctness, we mention that in general, the limit sets in the phase space with irrational rotation numbers can also be homeomorphic to Cantor sets (1-, 2-, or 3-Cantori) and this is even the "typical" case in some measure theoretic sense (Herman, 1983).

4.2 Bifurcations Within the Parameter Plane (μ, τ). We next investigate the activity patterns as a function of the connectivity number μ and the depression time constant τ (see Figure 9). From a phenomenological point of view, the possible oscillations we find for a pair of parameter values (μ, λ) are either in phase or, more frequently, antiphase. This behavior coincides well with the prediction of the local fixed-point analysis—with the fact that for $(|\lambda^-| < 1, |\lambda^+| > 1)$, an in-phase and for $(|\lambda^-| > 1, |\lambda^+| > 1)$ an antiphase solution emerge. By the same local analysis, the activity converges to the fixed point (P_{fix}, P_{fix}) if both eigenvalues have modulus smaller than 1 and the activity dies out if this fixed point does not exist at all. Thus, the classification of the fixed point yields the following criterion (cf. Figure 9):

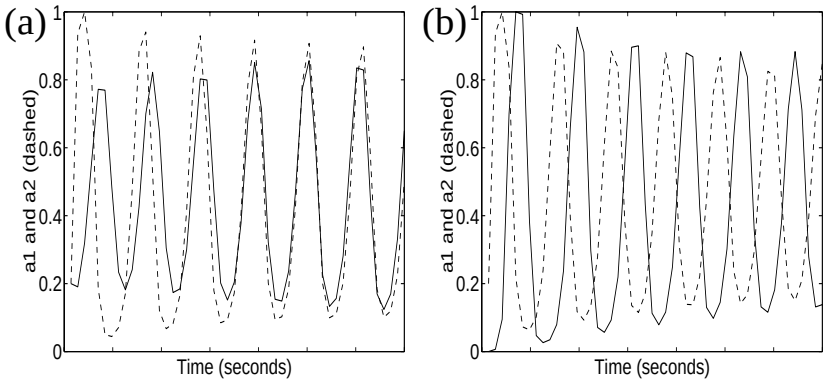

Figure 5: For particular parameter values ($\mu = 16$, $\tau = 9$, $\mu_{ij} = 0.1$, $K = 0.8$), the in-phase *and* the antiphase solutions are stable. This situation is possible only if the (pairwise complex conjugated) eigenvalues of the linearized mapping (see equation 2.4) at the fixed point have modulus greater than 1 ($|\lambda^-| = 1.012$, $|\lambda^+| = 1.019$). (a) With starting values $(a_0^1, s_0^1) = (0.2, 0.1)$ and $(a_0^2, s_0^2) = (0.2, 1)$, the activities synchronize. (b) With different starting values $(a_0^1, s_0^1) = (0, 1)$ and $(a_0^2, s_0^2) = (0.2, 1)$, the activities eventually lock antiphase.

Phenomenological criterion. *Let $\lambda^\pm$ be the eigenvalues (see equation 4.3) of the tangent mappings $d\phi^\pm$ restricted to the subspaces E^- and E^+. Then, the long-term behavior of the two network activities may be classified by*

1. no fixed point $\neq 0$: *extinction of both activities.*
2. $|\lambda^-| < 1$, $|\lambda^+| < 1$: *convergence of both to a constant activity $a_\circ \neq 0$.*
3. $|\lambda^-| < 1$, $|\lambda^+| > 1$: *stable in-phase oscillation.*
4. $|\lambda^-| > 1$, $|\lambda^+| > 1$: *typically a stable antiphase oscillation (if $|\lambda^-|$ and $|\lambda^+|$ are not too large, a stable in-phase solution may coexist).*

The criterion explains the dynamical behavior in Figure 8b where a change of the synaptic depression time τ from 4 to 10 and from 10 to 15 evoked the transition from convergence to in-phase oscillation and eventually to antiphase oscillation. For $\tau = 4$ we calculated $|\lambda^-| = 0.939 < 1$ and $|\lambda^+| = 0.950 < 1$ (convergence); for $\tau = 10$ we calculated $|\lambda^-| = 0.995 < 1$ and $|\lambda^+| = 1.005 > 1$ (in-phase oscillation) and for $\tau = 15$ we obtained $|\lambda^-| = 1.011 > 1$ and $|\lambda^+| = 1.021 > 1$ (antiphase oscillation).

The regions of the two-dimensional bifurcation diagram for the coupled networks almost coincide with the one for the isolated network (Senn et al., 1996). Whenever the activity of the isolated network dies out, converges, or oscillates, so do the activities of the coupled network. The in-phase oscillations occur only in a narrow strip of parameter values ($|\lambda^-| < 1$ and $|\lambda^+| > 1$)

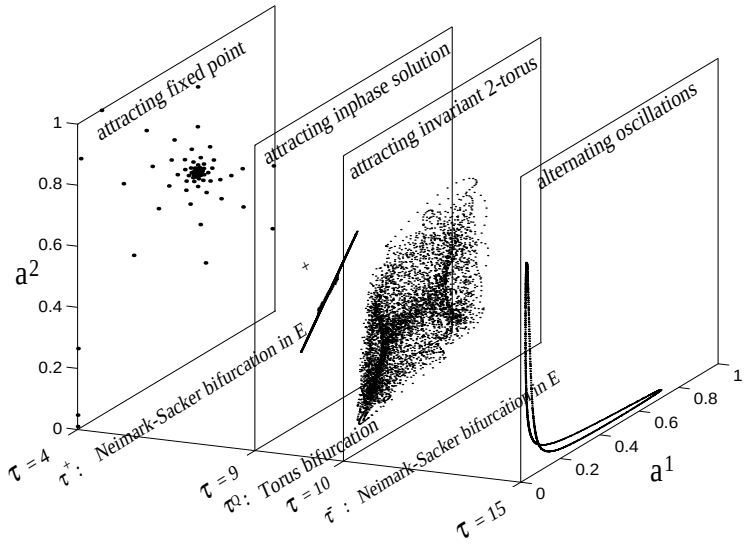

Figure 6: Orbits in the (a^1, a^2)-plane for different values of the synaptic depression time. The connectivity parameters are $\mu = 10$ and $\mu_{ij} = 0.1$. A time plot of the corresponding activities is shown in Figure 8b, and in Figure 4b, the full bifurcation diagram is depicted.

at the borderline between converging activity ($|\lambda^-| < 1$ and $|\lambda^+| < 1$) and antiphase oscillations ($|\lambda^-| > 1$ and $|\lambda^+| > 1$) (cf. Figure 9).

4.3 Estimating the Frequencies. In a first-order approximation, the frequencies f, f^+, and f^- of the uncoupled, the in-phase, and antiphase oscillations can be identified by those of the linearization at the fixed point—that is, by the rotation angles of the mappings $d\Phi^\circ$, $d\Phi^+$, and $d\Phi^-$, respectively. Here, $d\Phi^\circ$ represents the linearization of the uncoupled system with $\mu_{ij} = 0$ at the corresponding fixed point $\bar{P}_{fix} = (\bar{a}_\circ, \bar{s}_\circ)$. Using the abbreviation $\bar{\eta} = f_K(\mu\bar{a}_\circ\bar{s}_\circ)$ and $\eta = f_K((\mu + \mu_{ij})a_\circ s_\circ)$, we obtain the following relation for the linearized frequencies (cf. section A.3):

Lemma 1.

$$\cos(2\pi f) = \frac{\mu\bar{\eta}\bar{s}_\circ + \epsilon_\tau(1 - \epsilon_\tau\bar{a}_\circ)}{\sqrt{\mu\bar{\eta}\epsilon_\tau(\bar{s}_\circ + (1 - \epsilon_\tau)\bar{a}_\circ)}}$$

and

$$\cos(2\pi f^\pm) = \frac{(\mu \pm \mu_{ij})\eta s_\circ + \epsilon_\tau(1 - \epsilon_\tau a_\circ)}{\sqrt{(\mu \pm \mu_{ij})\eta\epsilon_\tau(s_\circ + (1 - \epsilon_\tau)a_\circ)}}.$$

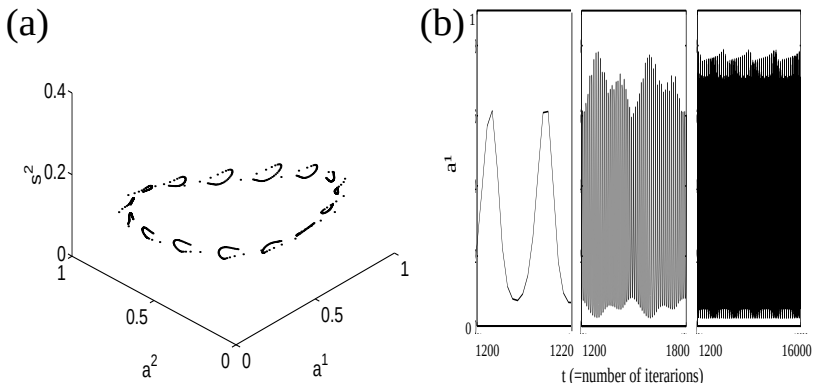

Figure 7: (a) A quasiperiodic orbit with two frequencies lies on a 2-torus generated by 5000 iterations of equation 2.4. Notice that the trajectory jumps clockwise from one circle to the next. The small circles correspond to the slow-amplitude oscillations. ($\mu = 10$, $\tau = 11$, $\mu_{ij} = .1$.) (b) In a quasiperiodic solution, two or more frequencies are involved at different timescales. The activity a^1 is shown during intervals of 20, 600, and 1480 iterations. ($\mu = 10$, $\tau = 12$, $\mu_{ij} = .1$.)

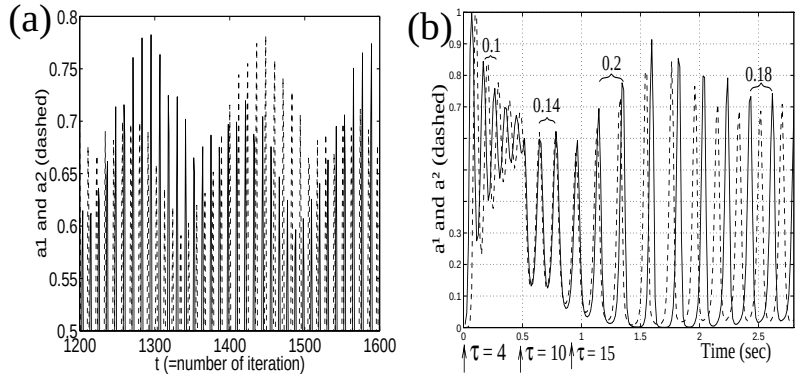

Figure 8: (a) Plotting the oscillations from the first network shown in Figure 7b (solid line) together with the oscillations of the second network (dashed line) reveals a quasiperiodic solution that is phase trapped. (b) While increasing the synaptic depression time τ, the dynamics change from convergence to a constant activity ($\tau = 4$, $t = 0, \ldots, 0.5$ s), to stable in-phase oscillation ($\tau = 10$, $t = 0.5, \ldots, 0.8$ s), and eventually to stable antiphase oscillation ($\tau = 15$, $t = 1, \ldots, 3$ s). The numbers in the figure give the period lengths of the oscillations in seconds. (Other parameter values: $\mu = 10$ and $\mu_{ij} = 0.1$.)

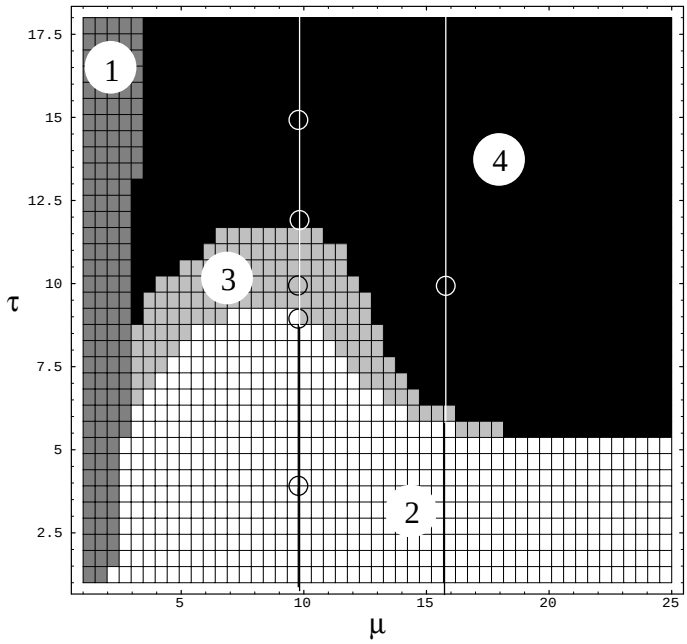

Figure 9: The four regions in the parameter space (μ, τ) for which the phenomenological criterion in section 4.2 predicts the following behavior: (1) extinction of any activity, (2) convergence to the constant activity $a_\circ$, (3) stable in-phase oscillations, and (4) typically stable alternating oscillations. Superimposed are the two lines corresponding to the running parameter in the bifurcation diagrams of Figure 4, and the circles refer to the parameter values chosen in Figures 5–8. The four different gray levels are determined by the evaluating formula (see equation 4.3). (Other parameters: $K = .8$, $\mu_{ij} = .1$.)

Evaluating these formulas for $\mu_{ij} = 0.1$ and for the parameters (μ, τ) with values lying in the domain $(1 \leq \mu \leq 25\,,\ 1 \leq \tau \leq 18)$ of Figure 9, one finds the relation $f < f^+ < f^-$. This confirms the frequency differences we measured in the case that both the in-phase and the antiphase solutions are stable (see Figure 10a): coupling the two oscillators with medium strength increases the frequencies of the oscillators, and the increase is larger for antiphase oscillations than for in-phase oscillations. That the antiphase oscillation is faster than the in-phase oscillation can also be seen by laying the in-phase and antiphase planes E^+ and E^- above each other and tracing two points on the invariant in-phase and antiphase curve C^+ and C^-, respectively (see Figure 10b). After 10 iterations, the point on the antiphase curve is moved by an angle $\triangle\theta$ farther to the right than the corresponding point on the in-phase curve. The validity of the inequality $f^+ < f^-$ is restricted

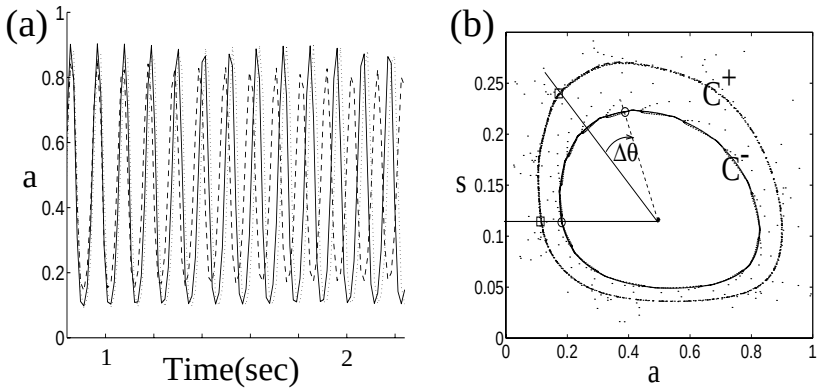

Figure 10: (a) One (in-phase) solution from Figure 5a (solid curve, frequency f^+), one (antiphase) solution from Figure 5b (dashed curve, frequency f^-), and the uncoupled solution (dotted curve, frequency f) are plotted for $t = 0, \ldots, 2.2$ s. As predicted by the local fixed-point analysis (section 4), we find $f < f^+ < f^-$. (b) Corresponding plots in the phase plane (a, s). The in-phase oscillations with larger amplitudes correspond to the outer invariant circle C^+, while the inner invariant circle C^- corresponds to the antiphase oscillations. After 10 iterations (≈ 0.14 s) the "in-phase" and "antiphase" map turned the square and the circle on the horizontal line onto the upper square and circle, respectively. A point on the inner antiphase curve is therefore turned by an angle $\triangle\theta$ "faster" to the right than a point on the outer in-phase curve. This again shows that $f^+ < f^-$.

by the following condition (which, however, is satisfied for the considered parameter values):

Theorem 2. *Let f^+ and f^- be the frequencies of the linearized in-phase and antiphase solutions. Then for small $\mu_{ij} > 0$, one has $f^+ < f^-$ if and only if $\epsilon_\tau \frac{1-a_\circ \epsilon_\tau}{s_\circ} < \mu\eta$.*

We emphasize that the theorem makes a statement about the frequencies of the linearized mapping at the fixed point. The interesting point is that these linearized frequencies fit the relation for the true frequencies in the case of medium-strength coupling (but not necessarily in the case of weak coupling). If we ask how these frequencies change with parameters μ and τ, we find that the frequencies do not change as long as the ratio μ/τ is constant. Increasing the average number of connections μ within each network accelerates the oscillations by the same factor as it does by decreasing the synaptic depression time. That this statement holds fairly well can be seen from Figure 4 in Senn et al. (1996), where both frequencies were plotted as functions of the parameters μ and τ. The decrease in frequency when the

synaptic depression time becomes longer can be seen in Figure 8b. The frequencies corresponding to the values $\tau = 4$, 10, 15 are 10 Hz, 7.1 Hz, and 5.6 Hz, respectively. Notice that for $\tau = 15$, the in-phase frequency during the short transition time is 5 Hz, which is indeed smaller than the antiphase frequency of 5.6 ($\approx 1/.18$) Hz after the transient. This is exactly what the theorem predicts.

5 Summary and Discussion

We have investigated the oscillation types of two weakly connected time-discrete networks induced by synaptic depression. The parameters that determine the oscillation pattern are not only the coupling strength between the networks but also the degree of connectivity among an individual network and the dynamics of the synaptic depression. By developing a discrete version of the APD theory, we showed that for weak coupling ($\mu_{ij} \sim 10^{-4}\mu$), an increase in the coupling strength can change a stable antiphase oscillation into a stable in-phase oscillation. For medium-strength coupling ($\mu_{ij} \sim 10^{-2}\mu$), we further encountered quasiperiodic oscillations for which the amplitude itself oscillates. In addition, stable in-phase *and* antiphase solutions for the same parameter values may coexist. A bifurcation analysis with respect to increasing synaptic depression time showed that from a rest point, an in-phase solution emerges through a Naimark-Sacker bifurcation. This inphase solution evolves to a quasiperiodic solution through a torus bifurcation. The phase lag changes from inphase to out of phase, and eventually a stable antiphase oscillation establishes itself. From a local fixed-point analysis, we deduced that coupling two oscillating networks generally increases the frequency; in case of bistability, the antiphase frequency is again higher than the in-phase frequency.

The transition from in-phase oscillations to antiphase oscillations is in our case either induced by increasing the synaptic depression time constant or decreasing the coupling strength between the networks. Roughly, *increasing* the depression time constant has the same effect on the dynamical behavior as *decreasing* the coupling strength. This is also true if one considers the change of frequency as a function of either the synaptic depression time or the coupling strength: increasing the synaptic depression time and decreasing the coupling strength between the networks lower the frequency (of the linearization at the fixed point (cf. Senn et al., 1996, Figure 4). This supports the suggestion of Kopell (1988) that physiological oscillators always speed up with excitatory input.

In our situation, an increase of the depression time constant destabilizes the in-phase oscillations. Destabilization of synchrony is also known to occur for increasing axonal delays (Crook, Ermentrout, Vanier, & Bower, 1997) or when increasing the rise time of the excitatory synaptic connections (van Vreeswijk, Abbott, & Ermentrout, 1994; Hansel, Mato, & Meunier, 1995). On the other hand, it is well known that for increasing coupling strength

between two oscillators, an antiphase oscillation will turn into an in-phase oscillation (Schillen & König, 1991; Sherman & Rinzel, 1992). This feature is used to train networks with a Hebbian learning rule to perform memory tasks (Horn & Usher, 1991) or to solve the binding problem (Wang & Terman, 1997). Our investigation suggests that these same tasks can be realized by learning the synaptic depression time constant where instead of a Hebbian increase of the coupling strength, the depression time constant of a synapse showing coincident presynaptic and postsynaptic activity is decreased. Such a network of oscillators based on depressing synapses would have the advantage of allowing for a richer dynamical behavior than a classical oscillator network based on pairs of excitatory and inhibitory cells with static synapses. (Note that one excitatory cell with N depressing synapses projecting onto it would correspond to one excitatory cell with N static synapses together with N inhibitory cells, which would regulate the response of these synapses.) It remains to be explored whether this additional dynamic complexity may improve the capacity of an oscillatory-based associative memory in storing spatiotemporal patterns.

For locomotion, traditional pattern generators are based on the idea that different activity patterns are induced by either tuning the coupling strength between the networks or changing the network configuration through central input (Grillner, 1981; Kopell, 1988). This study, however, suggests that spinal pattern generators may consist as well of unstructured excitatory neural networks characterized solely by the dynamics of their synaptic depression. The fact that different oscillatory behavior can emerge by changing the parameters of the synaptic depression opens the possibility of an activity-dependent self-regulation of the pattern generator. In order to test this hypothesis experimentally, we have started to perform multisite recordings of weakly coupled dissociated spinal networks and hope to be able to modulate the dynamics of synaptic depression at the different sites pharmacologically.

Appendix

A.1 Calculation of the Function $H(\phi)$. We assume that the uncoupled system has an invariant closed curve C° with irrational rotation number and first want to transform C° to a circle with constant rotation angle ω (in Figure 10, this curve coincides approximately with C^+). According to Denjoy theory, such a transformation is possible if the mapping on the invariant curve is at least twice continuously differentiable (Guckenheimer & Holmes, 1990); it may not be possible if the mapping is less smooth (Herman, 1983). Let α_t be the cumulated angle of an iterated point measured with respect to some zero direction and center P_{fix}. Since the mapping on the curve C° is injective and continuous (and thus monotonic), the average rotation angle $\omega = \lim_{t\to\infty} \alpha_t/t$ is well defined, and $\omega/2\pi$ represents the rotation number.

The transform $\alpha_t \overset{g}{\mapsto} \theta_t$ of α to the new angle coordinate θ with constant rotation is now defined by

$$\theta_t = g(\alpha_t) = t\omega \bmod 2\pi \qquad (t = 0, 1, 2, \ldots) \; . \tag{A.1}$$

Numerically this is done by iterating the uncoupled mapping (see equation 2.4) to obtain the list of angles $(\alpha_0, \alpha_1, \alpha_2, \ldots, \alpha_N) \bmod 2\pi$ and by assigning this list to the equidistant new angles $(0, \omega, 2\omega, \ldots, N\omega) \bmod 2\pi$. Continuous continuation leads to a coordinate transform $\alpha(\bmod 2\pi) \leftrightarrow \theta$ of the circle onto itself with the property in equation A.1 and which is again continuous and monotonic. All calculations were performed by MATLAB[1] and to implement the function F_K we used the built-in function *gammainc*.

Next we consider the two weakly coupled oscillators: the first at phase θ^1 and the second at phase θ^2 in the new angle coordinates. We define the function $h(\theta^1, \theta^2)$ as the deviation from the constant rotation angle ω of the first oscillator for one iteration step, which is caused by the coupling. Thus, setting $\theta_t^i := \theta^i$ for $i = 1, 2$, we calculate θ_{t+1}^1 in the presence of the coupling via $(\theta_t^1, \theta_t^2) \mapsto (\alpha_t^1, \alpha_t^2) \mapsto (\alpha_{t+1}^1, \alpha_{t+1}^2) \mapsto (\theta_{t+1}^1, \theta_{t+1}^2)$ and put $h(\theta^1, \theta^2) := \theta_{t+1}^1 - (\theta_t^1 + \omega)$ (while taking care of the 2π periodicity). To obtain $H(\phi)$ we calculate a list $h(\theta, \theta + \phi)$, $\theta \in [0, 2\pi]$, and average $h(\theta, \theta + \phi)$ over one cycle of θ (cf. equation 3.3).

A.2 The Local Fixed-Point Analysis. We consider the mapping (see equation 2.4) within the diagonalized coordinates (4.1), Φ: $(a_t^+, s_t^+, a_t^-, s_t^-) \longmapsto (a_{t+1}^+, s_{t+1}^+, a_{t+1}^-, s_{t+1}^-)$, and calculate its linearization at the fixed point $(P_{fix}, \mathbf{0})$, $P_{fix} = (a_\circ, s_\circ)$. We make the ansatz

$$\begin{aligned} a_t^1 &= a_\circ + \alpha_t \; , \qquad & a_t^2 &= a_\circ \pm \alpha_t \; , \\ s_t^1 &= s_\circ + \sigma_t \; , \qquad & s_t^2 &= s_\circ \pm \sigma_t \; , \end{aligned}$$

and consider the mapping $(\alpha_t, \sigma_t) \longmapsto (\alpha_{t+1}, \sigma_{t+1})$ in the two cases $\pm$. Writing the derivative of Φ at the fixed point according to equation 4.2, one obtains

$$\begin{aligned} d\Phi^\pm &= \begin{pmatrix} \frac{\partial a_{t+1}^\pm}{\partial a_t^\pm} & \frac{\partial a_{t+1}^\pm}{\partial s_t^\pm} \\ \frac{\partial s_{t+1}^\pm}{\partial a_t^\pm} & \frac{\partial s_{t+1}^\pm}{\partial s_t^\pm} \end{pmatrix} = \begin{pmatrix} \frac{\partial \alpha_{t+1}}{\partial \alpha_t} & \frac{\partial \alpha_{t+1}}{\partial \sigma_t} \\ \frac{\partial \sigma_{t+1}}{\partial \alpha_t} & \frac{\partial \sigma_{t+1}}{\partial \sigma_t} \end{pmatrix} \\ &= \begin{pmatrix} (\mu \pm \mu_{ij})\eta s_\circ & (\mu \pm \mu_{ij})\eta a_\circ \\ -\epsilon_\tau d_\tau (1 - s_\circ) & \epsilon_\tau d_\tau (a_\circ) \end{pmatrix}, \end{aligned} \tag{A.2}$$

where we used the abbreviations from equations 2.2 and 4.4. Now one makes use of the fact that the eigenvalues of $d\Phi^+$ and $d\Phi^-$ are complex conjugated.

[1] MATLAB, The Language of Technical Computing, MathWorks Inc., Version 2 (1996), http://www.mathworks.com.

This follows from the fact that $d\Phi^{\pm}$ is composed of a genuine rotation (cf. proof of lemma 2 in Senn et al., 1996). Let us denote the eigenvalues of $d\Phi^{+}$ and $d\Phi^{-}$ by $\lambda^{+}, \overline{\lambda^{+}}$, and $\lambda^{-}, \overline{\lambda^{-}}$, respectively. Their modulus can be calculated directly by means of the determinant, without knowing $\lambda^{\pm}$ explicitly:

$$|\lambda^{\pm}|^2 = \det\left(d\Phi^{\pm}\right) = (\mu \pm \mu_{ij})\eta\epsilon_\tau(s_\circ + (1-\epsilon_\tau)a_\circ)\ . \tag{A.3}$$

A.3 Proof of Lemma 1 and Theorem 2. Identifying the frequencies f, f^{+}, and f^{-} of the uncoupled, in-phase, and antiphase oscillations with those of the corresponding linearization, we have

$$\lambda = |\lambda| e^{i2\pi f}, \quad \lambda^{\pm} = |\lambda^{\pm}| e^{i2\pi f^{\pm}}, \tag{A.4}$$

where λ, λ^{+}, and λ^{-} are eigenvalues of $d\Phi^{\circ}$, $d\Phi^{+}$, and $d\Phi^{-}$, respectively. (We assume that $f,\ f^{\pm} > 0$; otherwise we take the complex conjugate of the eigenvalues.) The formula in the lemma for $\cos(2\pi f^{\pm})$ is obtained according to

$$\cos(2\pi f^{\pm}) = \frac{\mathrm{Re}(\lambda^{\pm})}{|\lambda^{\pm}|} = \frac{\mathrm{trace}(d\Phi^{\pm})}{2|\lambda|} = \frac{(\mu \pm \mu_{ij})\eta s_\circ + \epsilon_\tau d_\tau(a_\circ)}{\sqrt{(\mu \pm \mu_{ij})\eta\epsilon_\tau(s_\circ + (1-\epsilon_\tau)a_\circ)}}\ .$$

The first equality follows from equation A.4. The fact that the real part of $\lambda^{\pm}$ is half the trace of $d\Phi^{\pm}$ follows from the fact that $d\Phi^{\pm}$ is composed of a genuine rotation (Senn et al., 1996) and thus has the complex conjugated eigenvalues $\lambda^{\pm}$ and $\overline{\lambda^{\pm}}$ in their Jordan normal form. The trace of $d\Phi^{\pm}$ is read from equation A.2, and with equation A.3, we obtain the third equality. The formula for $\cos(2\pi f)$ is obtained in the same way.

To prove theorem 2, we must show the equivalence of $f^{-} < f^{+}$ and $\epsilon_\tau \frac{1-a_\circ\epsilon_\tau}{s_\circ} < \mu\eta$ for small μ_{ij}. According to Lemma 3 in Senn et al. (1996), the period of the uncoupled system is ≥ 4 and therefore the rotation angle ω is less than $\pi/2$. Thus, the relation $f^{-} < f^{+}$ is equivalent to $\cos(2\pi f^{-}) < \cos(2\pi f^{+})$, and by the lemma we get

$$\frac{(\mu - \mu_{ij})\eta s_\circ + \epsilon_\tau d_\tau(a_\circ)}{\sqrt{1 - \frac{\mu_{ij}}{\mu}}} < \frac{(\mu + \mu_{ij})\eta s_\circ + \epsilon_\tau d_\tau(a_\circ)}{\sqrt{1 + \frac{\mu_{ij}}{\mu}}}.$$

If we apply the binomial expansion

$$\frac{1}{\sqrt{1 \pm \frac{\mu_{ij}}{\mu}}} = 1 \mp \frac{\mu_{ij}}{2\mu} + O\left(\frac{\mu_{ij}}{\mu}\right)^2,$$

the first-order term μ_{ij}/μ cancels and, neglecting higher-order terms, the relation transforms after some algebraic manipulations to $\epsilon_\tau d_\tau(a_\circ) < \mu\eta s_\circ$.

Acknowledgments

W. S. and K. W. were supported by Swiss National Science Foundation grant 5002-03793 (Schwerpunktprogramm Biotechnologie), and J. K. was supported by grant 31-42055.94. We thank H.-P. Clamann for helpful comments and for correcting the English.

References

Abbott, L., Varela, J., Sen, K., & Nelson, S. (1997). Synaptic depression and cortical gain control. *Science, 275*, 220–224.

Arnold, V. I. (1965). Small denominators, I: Mappings of the circumference onto itself. *Am. Math. Soc. (AMS) Transl. Ser. 2, 46*, 213–284.

Collet, P., & Eckmann, J.-P. (1986). *Iterated maps on the interval as dynamical systems* (2nd ed.). Basel: Birkhäuser Verlag.

Crook, S., Ermentrout, G., Vanier, M., & Bower, J. (1997). The role of axonal delay in the synchronization of networks of coupled cortical oscillators. *J. Comput. Neuroscience, 4*, 161–172.

Ermentrout, G., & Kopell, N. (1991). Multiple pulse interactions and averaging in systems of coupled neural oscillators. *J. Math. Biol., 29*, 195–217.

Gao, B., & Ziskind-Conhaim, L. (1995). Development of glycine- and GABA-gated currents in rat spinal motoneurons. *J. Neurophysiol., 74*, 113–121.

Gerstner, W., Ritz, R., & van Hemmen, J. (1993). A biologically motivated and analytically soluble model of collective oscillations in the cortex. I. Theory of weak locking. *Biol. Cybernetics, 68*, 363–374.

Getting, P. (1989). Emerging principles governing the operation of neural networks. *Ann. Pew. Neurosci., 12*, 184–204.

Grillner, S. (1981). Control of locomotion in bipeds, tetrapods, and fish. In V. B. Brooks (Ed.), *Handbook of physiology, section 1: The nervous system* (Vol. 2, pp. 1179–1236). Bethesda, MD: American Physiological Society.

Guckenheimer, J., & Holmes, P. (1990). *Nonlinear oscillations, dynamical systems, and bifurcations of vector fields* (3rd ed.). New York: Springer-Verlag.

Hansel, D., Mato, G., & Meunier, C. (1995). Synchrony in excitatory neural networks. *Neural Computation, 7*, 307–337.

Herman, M. (1983). Sur les courbes invariantes par les difféomorphismes de l'anneau. *Astérisque, 103/104*.

Hlawka, E. (1979). *Theorie der Gleichverteilung*. Mannheim: Bibliographisches Institut.

Horn, D., & Usher, M. (1991). Parallel activation of memories in an oscillatory neural network. *Neural Computation, 3*, 31–43.

Kawato, M., & Suzuki, R. (1980). Two coupled neural oscillators as a model of the circadian pacemaker. *J. Theor. Biol., 86*, 547–575.

Kopell, N. (1988). Toward a theory of modelling central pattern generators. In A. H. Cohen, S. Rossignol, & S. Grillner (Eds.), *Neural control of phytmic movements in vertebrates* (pp. 369–413). New York: Wiley.

Kronauer, R., Czeisler, C., Pilato, S., Moore-Ede, M., & Weitzman, E. (1982).

Mathematical model of the human circadian system with two interacting oscillators. *Am. J. Physiol., 242*, R3–R17.

Markram, H., & Tsodyks, M. (1996). Redistribution of synaptic efficacy between neocortical pyramidal neurons. *Nature, 382*, 807–810.

Rinzel, J., & Ermentrout, B. (1989). Analysis of neural excitability and oscillations. In C. Koch & I. Segev (Eds.), *Methods in neuronal modeling: From synapses to networks.* Cambridge, MA: MIT Press.

Schillen, T., & König, P. (1991). Stimulus-dependent assembly formation of oscillatory responses II: Desynchronization. *Neural Computation, 3*, 167–178.

Senn, W., Wyler, K., Streit, J., Larkum, M., Lüscher, H.-R., Mey, H., Müller, L., Steinhauser, D., Vogt, K., & Wannier, T. (1996). Dynamics of a random neural network with synaptic depression. *Neural Networks, 9*(4), 575–588.

Sherman, A., & Rinzel, J. (1992). Rythmogenetic effects of weak electrotonic coupling in neural models. *Neurobiology, 89*, 2471–2474.

Streit, J. (1993). Regular oscillations of synaptic activity in spinal networks in vitro. *J. Neurophysiol., 70*, 871–878.

Streit, J., & Senn, W. (1997). *The generation of oscillatory activity in simulated random excitatory neronal networks with synaptic depression.* Manuscript submitted for publication.

Streit, J., Spenger, C., & Lüscher, H.-R. (1991). An organotypic spinal cord-dorsal root ganglia-skeletal muscle coculture of embryonic rat. II. Functional evidence for the formation of spinal reflex arcs in vitro. *Europ. J. Neurosci., 3*, 1054-1068.

van Vreeswijk, C., Abbott, L., & Ermentrout, G. (1994). When inhibition not excitation synchronizes neural firing. *J. Comput. Neuroscience, 1*, 313–322.

Wang, D., & Terman, D. (1997). Image segmentation based on oscillatory correlation. *Neural Computation, 9*, 805–836.

Wever, R. (1972). Virtual synchronization towards the limits of the range of entrainment. *J. Theor. Biol., 36*, 119–132.

Williams, T., & Bowtell, G. (1997). The calculation of frequency-shift functions for chains of coupled oscillators, with application to a network of the lamprey locomotor pattern generator. *J. Comput. Neuroscience, 4*, 47–55.

Received August 29, 1996; accepted November 3, 1997.